

Nanoscale

Accepted Manuscript



This is an *Accepted Manuscript*, which has been through the Royal Society of Chemistry peer review process and has been accepted for publication.

Accepted Manuscripts are published online shortly after acceptance, before technical editing, formatting and proof reading. Using this free service, authors can make their results available to the community, in citable form, before we publish the edited article. We will replace this *Accepted Manuscript* with the edited and formatted *Advance Article* as soon as it is available.

You can find more information about *Accepted Manuscripts* in the [Information for Authors](#).

Please note that technical editing may introduce minor changes to the text and/or graphics, which may alter content. The journal's standard [Terms & Conditions](#) and the [Ethical guidelines](#) still apply. In no event shall the Royal Society of Chemistry be held responsible for any errors or omissions in this *Accepted Manuscript* or any consequences arising from the use of any information it contains.



Journal Name

ARTICLE

Substrate Co-Doping Modulates Electronic Metal-Support Interactions and Significantly Enhances Single-Atom Catalysis[†]

J. L. Shi,^a J. H. Wu,^b X. J. Zhao,^a X. L. Xue,^a Y. F. Gao,^{c,d} Z. X. Guo^{e,a*}, and S. F. Li^{*a}

Received 00th January 20xx,
Accepted 00th January 20xx

DOI: 10.1039/x0xx00000x

www.rsc.org/

Transitional metal nanoparticles or atoms deposited on appropriate substrates can lead to highly economical, efficient, and selective catalysis. One of the greatest challenges is to control the electronic metal-support interactions (EMSI) between the supported metal atoms and the substrate so as to optimize their catalytic performance. Here, from first-principles calculations, we show that an otherwise inactive Pd single adatom on TiO₂(110) can be tuned into a highly effective catalyst, e.g. for O₂ adsorption and CO oxidation, by purposefully selected metal-nonmetal co-dopant pairs in the substrate. Such an effect is proved here to result unambiguously from a significantly enhanced EMSI. A nearly linear correlation is noted between the strength of the EMSI and the activation of the adsorbed O₂ molecule, as well as the energy barrier for CO oxidation. Particularly, the enhanced EMSI shifts upward the frontier orbital of the deposited Pd atom and largely enhances the hybridization and charge transfer between the O₂ molecule and Pd atom. Upon co-doping, the activation barrier for CO oxidation on the Pd monomer is also reduced to a level comparable to that on the Pd dimer which was experimentally reported to be highly efficient for CO oxidation. The present findings shed new insights into the understanding of the EMSI in heterogeneous catalysis and can open new avenue to design and fabrication of cost-effective single-atom-sized and/or nanometer-sized catalysts.

Introduction

Transitional metal (TM) and noble metal (NM) nanoparticles supported on oxide surfaces have been extensively used as efficient and economical catalysts in many industrial applications, such as CO oxidation in vehicle emission reduction,¹⁻³ Water-gas shift reaction,⁴ and hydrogenation.⁵ However, the intrinsic catalytic activities and selectivity of these supported metal particles are strongly size- and geometry-dependent, particularly at nanometer and sub-nanometer scales. In such regimes, the catalysis of TMs/NMs even with a given shape is characterized by a significant size effect, due to the variation of the increasingly large fraction of the low-coordinate metal atoms that often function as active sites for catalysis.⁶⁻⁸ As the ultimate size limit, single-atom catalysts (SAC) deposited uniformly on appropriate substrates, are widely expected to maximize the efficiency, activity and selectivity of TM and NM catalysts, particularly for the latter.

For example, SACs of Pt, Rh, Pd and Ru on FeO_x are reported to exhibit high performance for O₂ activation and CO oxidation.⁹ Fe single atom embedded in a silica matrix enhances methane activation.¹⁰ However, it was also experimentally reported that the catalytic activity for CO oxidation is insignificant for single Pd atoms on TiO₂(110), but is substantially higher for Pd ad-dimers and larger adsorbed clusters.³ Similarly, Au monomers show negligible catalytic activity on TiO₂(110) for CO oxidation though Au single atoms exhibit excellent catalysis on other substrates.^{4,11}

Clearly, substrate also plays a crucial role in the chemical activity and selectivity of the deposited nanocatalysts,¹²⁻¹⁴ as first recognized by Tauster *et al.*¹³ in 1978, and now well known as the “strong metal-support interactions (SMSI)”. Recently, Bruix *et al.*¹⁴ provide an in-depth analysis of the effect of SMSI on the significantly enhanced activity of Pt particles on ceria in water-gas shift reactions. More specifically, Campbell¹⁵ coins the findings of Bruix and co-workers¹⁴ as “electronic metal-support interactions” (EMSI) manifested by the chemical bonding and associated charge transfer at the metal-support interface. Namely, the enhanced activity of the deposited particles may be essentially attributed to electronic perturbations that modify the electronic states of the deposited metal and improve their catalytic properties due to the EMSI. To demonstrate more convincingly the importance of EMSI in the activity of a metal catalyst, it is imperative to focus on SAC systems,¹⁶ which can unambiguously rule out other factors, such as electronic quantum size effect^{17,18} and structural sensitivity^{19,20} involved in nanoparticles. In Hu and

^a International Laboratory for Quantum Functional Materials of Henan, School of Physics and Engineering, Zhengzhou University, Zhengzhou, Henan 450001, China
Email: sflizzu@zzu.edu.cn

^b Department of Physics, Henan Institute of Education, Zhengzhou, 450046, China

^c Department of Materials Science and Engineering, University of Tennessee, Knoxville, Tennessee 37996, USA

^d Materials Science and Technology Division, Oak Ridge National Laboratory, Oak Ridge, Tennessee 37831, USA

^e Department of Chemistry, University College London, London WC1H 0AJ, UK

[†] Electronic Supplementary Information (ESI) available: Details on the simulation methods, additional data is presented in Figures S1-S5. See DOI: 10.1039/x0xx00000x

co-worker's recent experiment the role of EMSI is established by comparison of the activities of Ag-SACs on two types of supports but with different local geometric structures, which in some sense dilutes the pure electronic effect of the EMSI.

Here, using state-of-the-art first-principles calculations, we consider a Pd atom supported in the vicinity of the surface oxygen vacancy of the rutile $\text{TiO}_2(110)$, $\text{Pd@TiO}_2(110)$, as a representative SAC for CO oxidation, to establish the role of a pure electronic effect in the EMSI in controlling the catalysis of a given SAC. A comparative investigation was carried out for the catalysis of the $\text{Pd@TiO}_2(110)$ and those with metal-nonmetal co-dopant pairs in the sub-layer, while keeping the local geometric structure of the Pd atom almost constant. In contrast to Bruix's model catalyst, the present systems can mostly rule out the geometric effect of the substrates in identifying the "pure" electronic contribution to the EMSI effect. Intriguingly, a nearly linear correlation between the strength of the EMSI and the CO oxidation rate was established in the studied systems, i.e., the stronger the EMSI, the larger the CO oxidation rate.

Methods

Our DFT calculations²¹ were performed using Vienna *ab initio* simulation package (VASP)²² with the projector augmented wave (PAW)²³ method. For the exchange-correlation energy, we employed the generalized gradient approximation functional of Perdew-Burke-Ernzerhof.²⁴ Simulation details are presented in S1 of the ESI†.

Results and discussion

First of all, we confirm that the Pd single atom prefers to locate in the vicinity of the surface oxygen vacancy (V_o) site of the $\text{TiO}_2(110)$ surface, as deduced from both the energetics and low diffusion rates of the Pd atoms observed in experiment,²⁵ supported also by recent state-of-the-art first-principles calculations.²⁶ Based on this, the O_2 adsorption and CO oxidation process are re-examined by extensive additional calculations. The present results are in close agreement with previous calculations,²⁶ i.e., the O_2 molecule can only weakly adsorb on the $\text{Pd@TiO}_2(110)$ complex with an adsorption energy, i.e., $E_{\text{ads}}(\text{O}_2)=0.241$ eV, and the CO oxidation experiences a large activation barrier of 1.132 eV. Therefore, both the small binding energy and the large CO oxidation barrier together determine the low catalysis of the $\text{Pd@TiO}_2(110)$. For more details on the geometric structure of the $\text{Pd@TiO}_2(110)$ and the minimum energy path for CO oxidation on it, see Fig. S1†.

To optimize the chemical activity of the intrinsically inert $\text{Pd@TiO}_2(110)$, co-doping is invoked here to modulate the electronic structures of the $\text{TiO}_2(110)$ substrate and consequently tune the EMSI between the Pd metal atom and the co-doped substrates. It is widely accepted that the substitutional doping of binary oxide semiconductor is

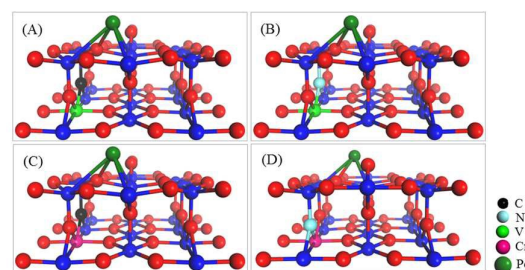


Fig.1 (Color online): Local geometric structures of co-doped $\text{Pd@TiO}_2(110)$ complexes with (A) V-C; (B) V-N; (C) Cr-C; and (D) Cr-N co-dopant pairs.

extremely difficult due to the limited solubility of the dopants, especially for *p*-type doping.²⁷ Recently, Zhu *et al.*²⁸ reported that the introduction of donor-acceptor co-dopant pairs is an effective approach in enhancing the solubility of dopants in TiO_2 . In view of this, we choose two typical 3*d* transition metals, V and Cr, as the *n*-type dopants to substitute for a Ti atom, and two nonmetal elements, N and C, as the *p*-type dopants to substitute for a neighboring O site, respectively. Therefore, four metal-nonmetal co-dopant pairs can be obtained, i.e., *p*-type V-C, compensated V-N and Cr-C, and *n*-type Cr-N, respectively.

Fig. 1 depicts the most stable configurations of the four co-doped $\text{Pd@TiO}_2(110)$ complexes. Energetically, it is confirmed that the co-dopant pairs do prefer to form a metal-nonmetal dimer in $\text{Pd@TiO}_2(110)$, due to the strong Coulombic electrostatic attraction between the metal donor and nonmetal acceptor ions. Consequently, the introduction of co-dopant pairs into the TiO_2 substrate leads to three important features for the binding of the Pd on the defective $\text{TiO}_2(110)$ surface. Firstly, without co-doping, the Pd atom favors exactly the V_o site, whereas it slightly departs from the V_o in the co-doped cases; however, upon O_2 and CO co-adsorption, the Pd atom on the pristine $\text{TiO}_2(110)$ also relaxes to the same local site as that in the co-doped cases, which will be discussed later; Secondly, as shown in Fig. 1, the Pd atom possesses similar local supporting structures in all the four co-doped cases, for details on the bond lengths of the Pd atom with the substrates, see S3 of the ESI†; Thirdly, the co-dopant pairs enhance the electronic binding of the Pd atom with the $\text{TiO}_2(110)$ substrate, i.e., from 1.641 to 1.788, 1.769, 1.768 and 1.768 eV, for the un-doped, V-C, V-N, Cr-C, and Cr-N co-doped $\text{Pd@TiO}_2(110)$, respectively.

Now, we discuss the doping effect in modulating the electronic structures of the Pd atom through EMSI. In Fig. 2, the total density of states (DOS) of the co-doped $\text{Pd@TiO}_2(110)$ species including the local projected DOS (LPDOS) of the dopants and the Pd atom are presented. For comparison, the LPDOS of the un-doped $\text{Pd@TiO}_2(110)$ are also shown in Fig. 2(A). As shown in Figs. 2(B)-(E), the energy gap between the valence band maximum (VBM) and the conduction band minimum (CBM) is significantly reduced by co-doping. Specifically, in the un-doped $\text{Pd@TiO}_2(110)$ system, the VBM is dominated by the *p* orbital of the O atoms and the CBM locates in the vicinity of the lowest-unoccupied-molecular-

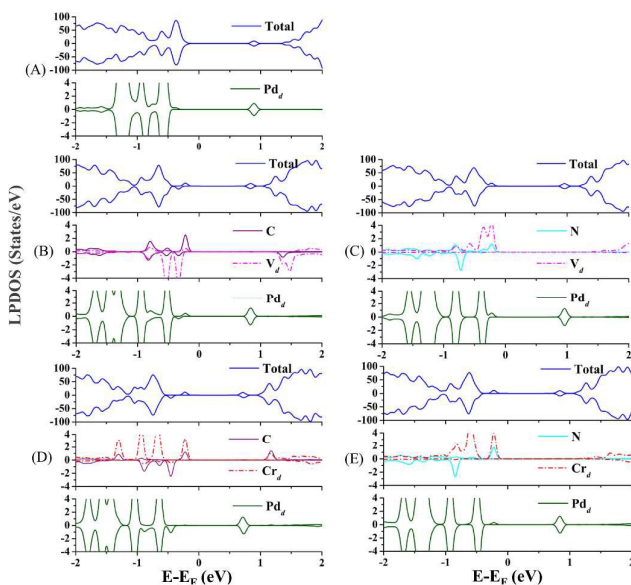


Fig. 2 (Color online): Total and local projected density of states (DOS) of (A): pristine rutile Pd@TiO₂(110); and that of (B): V-C, (C): V-N, (D): Cr-C and (E): Cr-N co-doped systems.

orbital (LUMO) of the Pd atom, respectively. In addition, the HOMO-LUMO gap ($E_{\text{gap}}(\text{HOMO-LUMO})$) of the Pd atom is about 1.464 eV. Upon doping, both the VBM and CBM are changed due to the introduction of the co-dopant states and the resulted EMSI. Distinctly, in all these four co-doped cases, the VBM is shifted upward and now positioned in the vicinity of the HOMO of the co-dopant pairs (see Figs. 2(B)-(E)), and the CBM is further lowered except for the cases of V-N co-doping (see Fig. 2(C)). Importantly, the frontier orbital (HOMOs) of the Pd atom hybridizes with the co-dopant states by the Fermi level, which effectively upward shifts the HOMOs of the Pd single atom. For example, in the *p*-type V-C co-doped complex, the (*d*-electron dominated) HOMOs of the Pd atom hybridizes with the HOMOs of V atom and those of the C atom in the energy window of -0.6 to -0.3 eV. Furthermore, the HOMO of the Pd atom is now upward shifted by about 0.5 eV, see Fig. 2(B). Moreover, such an orbital hybridization between the Pd atom and the substrate, particularly with the doped metal cations, is accompanied with charge transfer from the former to the latter via a charge compensation mechanism. Therefore, such a charge transfer leads the Pd atom to

Table I. Effect of Co-doping on the O₂ Activation by Pd@TiO₂(110). Calculated binding energy, $E_b(\text{Pd})$ and charge state $Q(\text{Pd})$ of the Pd single atom on pristine and co-doped rutile Pd@TiO₂(110) surfaces. The adsorption energy, $E_{\text{ads}}(\text{O}_2)$; O-O bond length, $R(\text{O-O})$; charge transfer, $Q(\text{O}_2)$ and the stretching vibrational frequency, ω of the lowest energy structures of an O₂ molecule adsorption on pristine and co-doped rutile Pd@TiO₂(110) surfaces.

Systems	$E_b(\text{Pd})(\text{eV})$	$Q(\text{Pd})(\text{e})$	$E_{\text{ads}}(\text{O}_2)(\text{eV})$	$R(\text{O-O})(\text{\AA})$	$Q(\text{O}_2)(\text{e})$	$\omega(\text{cm}^{-1})$
Pd@TiO ₂ (110): V-C	1.788	+0.161	0.808	1.275	0.22	1296.32
Pd@TiO ₂ (110): V-N	1.769	+0.160	0.732	1.274	0.21	1302.04
Pd@TiO ₂ (110): Cr-C	1.768	+0.164	0.794	1.278	0.22	1284.58
Pd@TiO ₂ (110): Cr-N	1.768	+0.162	0.801	1.277	0.23	1348.51
Pd@TiO ₂ (110)	1.641	+0.158	0.241	1.254	0.10	1560.83

departure from its closed-shell (d^{10}) characteristics, and it is now positively charged, as confirmed by the Bader charge analysis presented in Table I. Here, we emphasize that it is just the hybridization and charge transfer that raise the HOMO of the Pd atom and enhance its chemical activity towards oxygen adsorption and activation, which will be illustrated shortly.

Adsorption of O₂ molecules on co-doped Pd@TiO₂(110) SACs

To further identify the co-doping effect in modulating the chemical activity of the Pd atom via the EMSI, we now investigate the key process of CO oxidation, i.e., the adsorption and activation of an O₂ molecule on the co-doped structures presented in Fig. 1. Upon extensive calculations, we identified the most stable configurations for O₂ adsorption on the four co-doped Pd@TiO₂(110) complexes, as shown in Fig. 3. Note that in the optimized O₂-Pd@TiO₂(110) co-doped structures, the Pd atoms only binds directly with one oxygen atom of the O₂ molecule, which is very similar to the O₂ adsorption on other low dimensional noble metal structures.^{29, 30} In contrast to the case of the un-doped Pd@TiO₂(110), the O₂ molecule is found to bind strongly to the Pd atom deposited on the doped TiO₂(110) substrates. Specifically, as summarized in the Table I, the adsorption energy ($E_{\text{ads}}(\text{O}_2)$) of the O₂ molecule is increased from 0.241 to 0.808, 0.732, 0.794, and 0.801 eV, for the pristine Pd@TiO₂(110), the V-C, V-N, Cr-C, and Cr-N co-doped complexes, respectively. Meanwhile, in the V-C, V-N, Cr-C, and Cr-N co-doped cases, the stretching vibrational frequency of the adsorbed O₂ molecule is further red-shifted from 1560.83 to 1296.32, 1302.04, 1284.58, 1348.51 cm⁻¹, due to the enlarged O-O bond lengths, i.e., 1.275, 1.274, 1.278, and 1.277 Å, respectively. These data convincingly indicate that the O₂ molecule is considerably activated on these co-doped Pd@TiO₂(110) SAC due to the enhanced EMSI.

Now, we further explore the underlying mechanism of the EMSI in improving the chemical activity of the Pd atom via co-doping. In doing so, we analyze the DOS of the optimized final states of the O₂ molecule adsorbed on the Pd atom on TiO₂(110) co-doped by V-C, V-N, Cr-C, and Cr-N pairs, respectively. In Figs. 4(B)-(E), the LPDOS of all the Ti atoms, Pd atom, co-dopant pairs, and the adsorbed O₂ species are

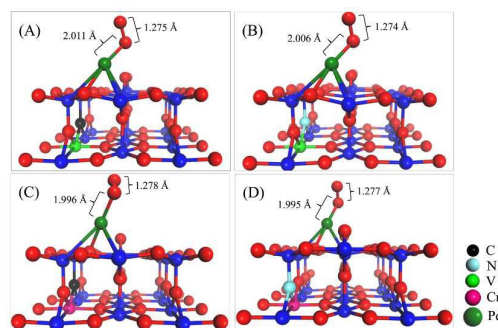


Fig. 3 (Color online): Geometric O₂ adsorption structures of co-doped Pd@TiO₂(110) complexes with (A) V-C; (B) V-N; (C) Cr-C; and (D) Cr-N co-dopant pairs.

presented. In addition, the DOS for O₂ on the un-doped Pd@TiO₂(110) is also comparatively shown in Fig. 4(A). Here, to illustrate more clearly the role of the EMSI, we only focus on an energy window of -2.0 to 2.0 eV by the Fermi level in analyzing the DOS. As shown in Fig. 4(A), for O₂ adsorption on the un-doped Pd@TiO₂(110), there is negligible hybridization between the HOMO of the deposited Pd atom and the LUMO of the O₂ molecule, due to the relatively deep energy level of the HOMO and the large E_{gap}(HOMO(Pd)-LUMO(O₂)). Therefore, O₂ can only weakly bind to the Pd@TiO₂(110) SAC with minor charge transfer obtained by Bader charge analysis, i.e., about 0.1 *e* from the Pd to the adsorbed O₂ species. However, upon co-doping, the *d*-electron dominated HOMO of the Pd atom hybridizes with that of the co-dopant pairs in the vicinity of the Fermi level. These hybridized filled states serve as an effective electron reservoir for the incoming O₂ molecule to capture the electron charge. More specifically, taking the O₂ adsorption on the Cr-N co-doped case as an example, one can see that though the Pd atom only slightly hybridizes with the HOMO (which is about 0.2 eV below the Fermi level) of the Cr atom, in the final state, such an orbital hybridization is significantly enhanced, see Fig. 4(E); meanwhile, for the adsorbed O₂ molecule there exists considerable spin-minority LPDOS hybridization with that of the Pd atom around 0.7 eV below the Fermi level. We emphasize that when the O₂ molecule is far away from the Pd atom, the spin-minority LPDOS (O₂) is about 1.2 eV above the Fermi level and totally unfilled. These results confirm an evident charge transfer (about 0.3 *e*) from the SAC to the O₂ molecule. Therefore, one can conclude that the *n*-type Cr-N pair (essentially the metal Cr) plays an important role in serving as the charge reservoir, compensating for the charge of the Pd atom, and thus enhancing the interaction with the O₂ molecule.

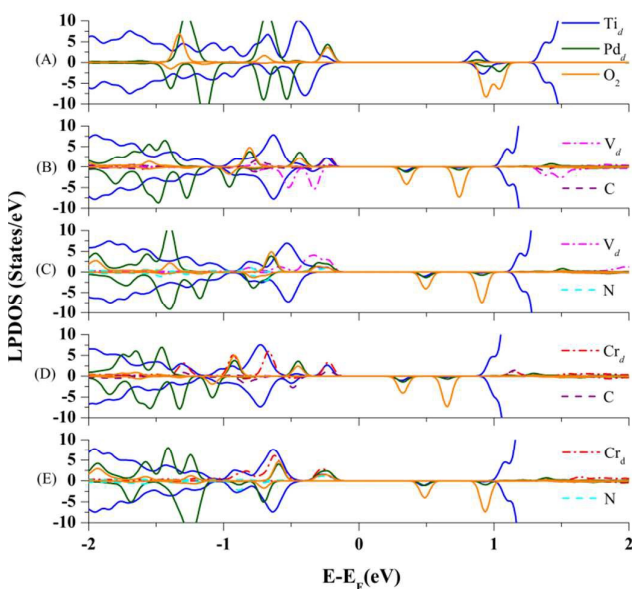


Fig. 4 (Color online): Local projected density of states of optimized structures for O₂ molecule adsorption on (A): pristine rutile Pd@TiO₂(110); and that of (B): V-C, (C): V-N, (D): Cr-C and (E): Cr-N co-doped complexes.

Subsequently, such a charge transfer weakens the O-O bond and further strengthens the O₂ activation as manifested by the enlarged E_{ads}(O₂) of 0.801 eV and red-shifted stretching vibration frequency of 1348.51 cm⁻¹, see Table I.

Note that the *p*-type V-C, and the two compensated V-N and Cr-C couplings also significantly facilitate the O₂ adsorption and activation via a similar mechanism due to the enhanced EMSI. As shown in Figs. 3(B), (C), and (D), the co-dopant-assisted enhanced hybridizations between the Pd atom and the O₂ molecule are also observed in the energy range of -1.0 to 1.0 eV by the Fermi levels. Such interactions stimulate the charge transfer between the O₂ molecule and SAC, and enhance the O₂ activation, as seen from the calculated data summarized in Table I. Based on the present findings, we can conclude that the chemical activity of the intrinsically inert Pd atom can be effectively optimized by the EMSI via co-doping approach. To further identify the dominated intrinsic parameter in such an optimization rule, we analyze the DOS of the O₂ molecule far (about 5.0 Å) above these co-doped Pd@TiO₂(110) SACs, including other *n*-type of co-doping, such as Cr-S pair, for details, see S4 of the ESI†. We find that, over all, the smaller the E_{gap}(HOMO(Pd)-LUMO(O₂)), the larger the E_{ads}(O₂), as presented in Fig. 5, in line with the well-known *d*-band theory.^{31, 32} Note again that, as presented in ESI† (S4) and the above discussion, the reduced E_{gap}(HOMO(Pd)-LUMO(O₂)) is originated from an enhanced EMSI through *n-p* co-doping, i.e., the stronger the EMSI, the smaller the E_{gap}(HOMO(Pd)-LUMO(O₂)); and consequently the stronger the O₂ activation.

CO oxidation on *n-p* co-doped Pd@TiO₂(110)

Having clearly illustrated the critical step of O₂ activation on the *n-p* co-doped Pd@TiO₂(110) systems, we continue to investigate the kinetic processes of CO oxidation on the improved Pd@TiO₂(110) SACs. Typically, taking the *p*-type V-C and *n*-type Cr-N co-doped cases as prototypical examples, we investigate the EMSI in optimizing CO oxidation rates by performing substantial simulations using the NEB method.³³

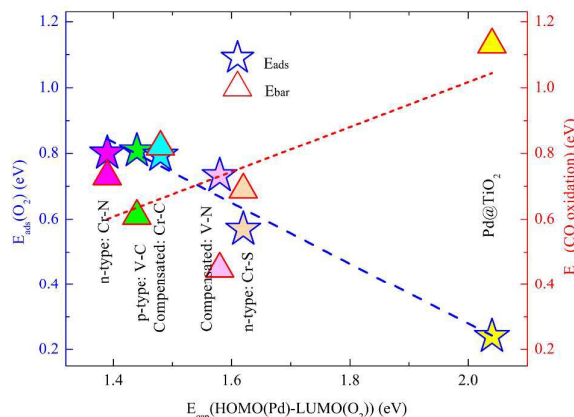


Fig. 5 (Color online): Adsorption energy of the O₂ molecule, E_{ads}(O₂) (Activation barrier for CO oxidation, E_{bar}(CO oxidation)) on Pd@TiO₂(110) and co-doped counterparts with V-C, V-N, Cr-C, Cr-N, and Cr-S co-dopant pairs.

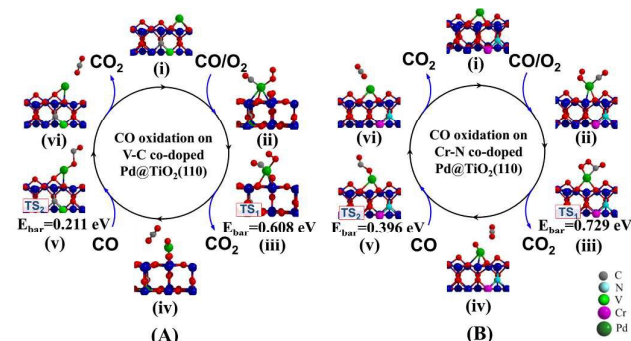


Fig. 6 (color online): Minimum energy paths for CO oxidation on Pd@TiO₂(110) co-doped with prototypical metal-nonmetal pairs. **(A)**: *p*-type V-C and **(B)**: *n*-type Cr-N co-dopants.

First, three CO oxidation mechanisms proposed by recent theoretical studies^{34, 35} have been re-examined in the present work. Interestingly, we confirm that the CO oxidation prefers the Langmuir–Hinshelwood (L-H) process in both cases, i.e., CO can also adsorb on the single Pd atom nearby the O₂ molecule and the co-adsorbed molecules undergo a bimolecular reaction through formation of a CO₂ precursor, and then releasing the CO₂ molecule upon further activations. Note also that for both the pristine and the co-doped Pd@TiO₂(110) complexes, upon CO and O₂ co-adsorption, the Pd atom locates in almost the same position close to the surface V_O site, see also the Fig. S1(B)† and Fig. 6. The detailed pathways and energetics for both cases are shown in Fig. 6. More specifically, as shown in Fig. 6(A), in the case of *p*-typed V-C co-doped Pd@TiO₂(110) system (see structure (i)), we find that the first CO molecule easily adsorbs in the vicinity of the O₂ molecule on the Pd catalyst (structure (ii)) via the well-known back-donation charge transfer mechanism,^{32, 36} i.e., donation of CO 5σ electrons to the Pd@TiO₂(110) substrate and back-donation from the Pd metal atom into the unoccupied 2π* orbital of CO. Here, we note that, as shown in Fig. 2, the upward shifted HOMO and slightly downward shifted LUMO orbitals of the Pd atom due to the enhanced EMSI promotes the back-donation process. Consequently, the bond length of the adsorbed CO species is slightly enlarged to 1.154 Å from 1.143 Å of the gas phase, and correspondingly the C-O vibrational frequency is red shifted to 2037.56 cm⁻¹ from 2120.64 cm⁻¹. Such a back-donation interaction effectively weakens the C-O bond strength and facilitates the formation of a bent CO₂ intermediate species when the CO molecule attacks the adsorbed O₂ species. Note that the modest activation of the CO as manifested by the red-shifted vibration frequency renders the Pd atom to be good SAC candidate in avoiding poisoning. An endothermic process with low activation barrier of E_{bar}=0.608 (see Fig. 6(A)-(iii)) for CO₂ formation and E_{bar}=0.182 eV for CO₂ desorption are observed, respectively. Furthermore, when the first CO molecule is oxidized to release a CO₂, as presented in Fig. 6(A)-(iv), on the Pd atom there is still one O atom left which can be directly attached by the second incoming CO molecule in formation of the second CO₂, i.e., via the Eley-Rideal (E-R) mechanism (see Fig. 6(A)-(v)), with

an activation barrier of only 0.211 eV. After that, a second round of O₂ activation and CO oxidation can be continued.

For the case of *n*-typed Cr-N co-doping, see Fig. 6(B)-(i), a slightly higher energy barrier of 0.729 eV (see structure (iii)) is detected for the first CO molecule oxidation via the L-H mechanism and 0.396 eV (see structure (v)) for the second CO molecule oxidation via E-R process, respectively. Such similar rate-determining kinetic processes of the CO oxidation in these two cases can be ascribed to the comparable O₂ activations, as indicated by the negligible differences in the E_{ads}(O₂) and enlarged O-O bond lengths, as well as the very close values of the red-shifted O-O vibrational frequencies. Here, we also emphasize that in the un-doped Pd@TiO₂(110), the large activation barrier for CO oxidation and the significantly small E_{ads}(O₂) together dominated the low catalysis of the Pd SAC in the vicinity of the V_O. However, the calculated enlarged E_{ads}(O₂)/E_{ads}(CO) of 0.808/0.705, 0.801/0.792, 0.794/0.606, and 0.732/0.443 eV on the *p*-type V-C, *n*-type Cr-N, compensated Cr-C, and compensated V-N co-doped Pd@TiO₂(110), along with the reduced E_{bar} of 0.608, 0.729, 0.822, 0.423 eV for CO oxidation render the Pd atom to be effective for CO oxidation on the same site as that in the un-doped TiO₂(110), demonstrating the crucial role of the EMSI in tuning the catalysis of the Pd atom. From Fig. 5, one can see that, the calculated values of the E_{bar} for the case of the pristine Pd@TiO₂(110) and those of five co-doped establish an overall linear scale behavior as a function of the HOMO(Pd)-LUMO(O₂) gap, except for the case of the V-N co-doping, which slightly departs from the fitted linear trend due to the relatively large energy gain upon the local geometric relaxation around the Pd single atom during the CO oxidation, see S5 of the ESI†. Importantly, we emphasize that an activation barrier of about 0.68 eV is calculated for CO oxidation on the Pd₂@TiO₂(110),²⁶ which was reported to possess good performance for CO oxidation in experiment.³ Therefore, the present results suggest that upon co-doping with low-cost metal-nonmetal pairs, the intrinsically inert noble Pd SAC is now expected to possess highly efficient catalysis for CO oxidation.

Conclusions

In conclusion, using state-of-the-art first-principles calculations, we performed a comparative study of the electronic structures of a Pd single ad-atom over a defective and metal-nonmetal co-doped TiO₂(110) substrates to establish the key role of the EMSI in optimizing the catalysis of SAC. Via the enhanced EMSI by co-doping, the intrinsically inert Pd atom on pristine TiO₂(110) can be tuned to serve as effective electron charge reservoir sustained by the hybridized states of the co-dopant pairs to facilitate O₂ activation and CO oxidation. Interestingly, a close-linear correlation between the strength of the EMSI and the activation of the adsorbed O₂ molecule, as well as the energy barrier for CO oxidation, is observed in the cases of Pd atom deposited on both pristine TiO₂(110) and co-doped substrates with low-cost metal-nonmetal pairs. The present findings shed new insights into

the understanding of the EMSI in heterogeneous catalysis and can open new avenue to design and fabrication of highly efficient and cost-effective single-atom- and/or nanometer-sized catalysts.

Acknowledgements

We thank Professor Jun-Hyung Cho and Professor Yu Jia, and Professor Zhenyu Zhang for helpful discussion. This work was supported by the NSFC (Grants No. 11074223, No. 11034006 and No. 11674289), and partly by the UK EPSRC (EP/L0183301/1) and US NSF (CMMI-1300223)

References

- B. Qiao, A. Wang, X. Yang, L. F. Allard, Z. Jiang, Y. Cui, J. Liu, J. Li and T. Zhang, *Nat. Chem.*, 2011, **3**, 634-641.
- M. Moses-DeBusk, M. Yoon, L. F. Allard, D. R. Mullins, Z. Wu, X. Yang, G. Veith, G. M. Stocks and C. K. Narula, *J. Am. Chem. Soc.*, 2013, **135**, 12634-12645.
- W. E. Kaden, T. Wu, W. A. Kunkel and S. L. Anderson, *Science*, 2009, **326**, 826-829.
- Q. Fu, H. Saltsburg and M. Flytzani-Stephanopoulos, *Science*, 2003, **301**, 935-938.
- G. Vilé, D. Albani, M. Nachtegaal, Z. Chen, D. Dontsova, M. Antonietti, N. López and J. Pérez-Ramírez, *Angew. Chem., Int. Ed.*, 2015, **54**, 11265-11269.
- N. Lopez, T. V. W. Janssens, B. S. Clausen, Y. Xu, M. Mavrikakis, T. Bligaard and J. K. Nørskov, *J. Catal.*, 2004, **223**, 232-235.
- H. Zhang, T. Watanabe, M. Okumura, M. Haruta and N. Toshima, *Nat. Mater.*, 2012, **11**, 49-52.
- L. Li, A. H. Larsen, N. A. Romero, V. A. Morozov, C. Glinsvad, F. Abild-Pedersen, J. Greeley, K. W. Jacobsen and J. K. Nørskov, *J. Phys. Chem. Lett.*, 2013, **4**, 222-226.
- F. Li, Y. Li, X. C. Zeng and Z. Chen, *ACS Catal.*, 2015, **5**, 544-552.
- X. Guo, G. Fang, G. Li, H. Ma, H. Fan, L. Yu, C. Ma, X. Wu, D. Deng, M. Wei, D. Tan, R. Si, S. Zhang, J. Li, L. Sun, Z. Tang, X. Pan and X. Bao, *Science*, 2014, **344**, 616-619.
- S. Lee, C. Fan, T. Wu and S. L. Anderson, *J. Am. Chem. Soc.*, 2004, **126**, 5682-5683.
- J. Zhang and A. N. Alexandrova, *J. Phys. Chem. Lett.*, 2013, **4**, 2250-2255.
- S. J. Tauster, S. C. Fung and R. L. Garten, *J. Am. Chem. Soc.*, 1978, **100**, 170-175.
- A. Bruix, J. A. Rodriguez, P. J. Ramirez, S. D. Senanayake, J. Evans, J. B. Park, D. Stacchiola, P. Liu, J. Hrbek and F. Illas, *J. Am. Chem. Soc.*, 2012, **134**, 8968-8974.
- C. T. Campbell, *Nat. Chem.*, 2012, **4**, 597-598.
- P. Hu, Z. Huang, Z. Amghouz, M. Makkee, F. Xu, F. Kapteijn, A. Dikhtiarenko, Y. Chen, X. Gu and X. Tang, *Angew. Chem., Int. Ed.*, 2014, **53**, 3418-3421.
- O. Lopez-Acevedo, K. A. Kacprzak, J. Akola and H. Häkkinen, *Nat. Chem.*, 2010, **2**, 329-334.
- M. Valden, X. Lai and D. W. Goodman, *Science*, 1998, **281**, 1647-1650.
- S. Dahl, A. Logadottir, R. C. Egeberg, J. H. Larsen, I. Chorkendorff, E. Törnqvist and J. K. Nørskov, *Phys. Rev. Lett.*, 1999, **83**, 1814-1817.
- J. K. Nørskov, T. Bligaard, B. Hvolbaek, F. Abild-Pedersen, I. Chorkendorff and C. H. Christensen, *Chem. Soc. Rev.*, 2008, **37**, 2163-2171.
- P. Hohenberg and W. Kohn, *Phys. Rev. B*, 1964, **136**, B864.
- G. Kresse and J. Hafner, *Phys. Rev. B*, 1994, **49**, 14251.
- P. E. Blochl, *Phys. Rev. B*, 1994, **50**, 17953.
- J. P. Perdew, K. Burke and M. Ernzerhof, *Phys. Rev. Lett.*, 1996, **77**, 3865.
- C. Xu, X. Lai, G. W. Zajac and D. W. Goodman, *Phys. Rev. B*, 1997, **56**, 13464-13482.
- S. Li, X. Zhao, J. Shi, Y. Jia, Z. Guo, J.-H. Cho, Y. Gao and Z. Zhang, *Phys. Chem. Chem. Phys.* (submitted, 2016).
- S. B. Zhang, *J. Phys.: Condens. Matter*, 2002, **14**, R881.
- W. Zhu, X. Qiu, V. Iancu, X.-Q. Chen, H. Pan, W. Wang, N. M. Dimitrijevic, T. Rajh, H. M. Meyer, M. P. Paranthaman, G. M. Stocks, H. H. Weitering, B. Gu, G. Eres and Z. Zhang, *Phys. Rev. Lett.*, 2009, **103**, 226401.
- H. Häkkinen, S. Abbet, A. Sanchez, U. Heiz and U. Landman, *Angew. Chem., Int. Ed.*, 2003, **42**, 1297-1300.
- I. N. Remediakis, N. Lopez and J. K. Nørskov, *Angew. Chem., Int. Ed.*, 2005, **44**, 1824-1826.
- B. Hammer, Y. Morikawa and J. K. Nørskov, *Phys. Rev. Lett.*, 1996, **76**, 2141-2144.
- L. P. A. Nilsson, and J. K. Nørskov., *Chemical Bonding at Surfaces and Interfaces*, (Elsevier, Amsterdam, 2008).
- G. Henkelman, B. P. Uberuaga and H. Jónsson, *J. Chem. Phys.*, 2000, **113**, 9901-9904.
- H. Y. Kim, H. M. Lee and G. Henkelman, *J. Am. Chem. Soc.*, 2012, **134**, 1560-1570.
- C. Zhang, A. Michaelides and S. J. Jenkins, *Phys. Chem. Chem. Phys.*, 2011, **13**, 22-33.
- R. Hoffmann, *Rev. Mod. Phys.*, 1988, **60**, 601-628.